Volume 48
Number 12
28 March 2024
Pages 5077–5556

NJC

New Journal of Chemistry

A journal for new directions in chemistry

rsc.li/njc

ISSN 1144-0546

ROYAL SOCIETY OF CHEMISTRY

PAPER

Petr Štěpnička *et al.*

Synthesis, reactivity and coordination behaviour of a ferrocene phosphinostibine and intramolecular interactions in its P(v) and Sb(v) derivatives

cnrs

NJC

ROYAL SOCIETY OF CHEMISTRY

PAPER

View Article Online
View Journal | View Issue

Cite this: *New J. Chem.*, 2024, **48**, 5107

Synthesis, reactivity and coordination behaviour of a ferrocene phosphinostibine and intramolecular interactions in its P(v) and Sb(v) derivatives†

Jakub Antala, Jiří Schulz, Ivana Císařová and Petr Štěpnička *

Received 22nd January 2024,
Accepted 13th February 2024

DOI: 10.1039/d4nj00349g

rsc.li/njc

Compared to their P,N-analogues, compounds combining P and Sb substituents remain less common. This contribution describes the synthesis of a new ferrocene phosphinostibine, $Cy_2PfcSbPh_2$ (**3**; fc = ferrocene-1,1′-diyl, Cy = cyclohexyl), and its derivatives modified at the phosphine and stibine moieties, *viz.*, $Cy_2P(E)fcSbPh_2$ (E = BH_3, O, S, AuCl), $Cy_2P(E)fcSbCl_2Ph_2$ (E = BH_3, S, AuCl) and stiboranes $Cy_2P(E)fcSb(O_2C_6Cl_4)Ph_2$ (E = void, BH_3, O, S and AuCl). The increased Lewis acidity of the Sb atom in the catecholatostiboranes $Cy_2PfcSb(O_2C_6Cl_4)Ph_2$ and $Cy_2P(O)fcSb(O_2C_6Cl_4)Ph_2$ resulted in intramolecular P → Sb and O → Sb dative interactions, which were not detected for the respective parent stibines or even in $Cy_2P(S)fcSb(O_2C_6Cl_4)Ph_2$. While the P → Sb interaction in $Cy_2PfcSb(O_2C_6Cl_4)Ph_2$ was stronger than that in the "all-phenyl" analogue $Ph_2PfcSb(O_2C_6Cl_4)Ph_2$ due to the electron-donating effect of the cyclohexyl groups, the bonding situations in $Cy_2P(O)fcSb(O_2C_6Cl_4)Ph_2$ and $Ph_2P(O)fcSb(O_2C_6Cl_4)Ph_2$, where the substituent effect was only indirect, remained very similar according to DFT calculations. A coordination study with **3** resulted in isolation of phosphine ([AuCl(**3**-κP)]), P,Sb-bridging ([(μ(P,Sb)-**3**)$(AuCl)_2$]), and P,Sb-chelate ([(arene)MCl(**3**-κ^2P,Sb)]X, where (arene)M/X = (η^6-*p*-cymene)Ru(II)/PF_6, (η^5-C_5Me_5)Rh(III)/Cl, and (η^5-C_5Me_5)Rh(III)/PF_6, and [MCl_2(**3**-κ^2P,Sb)], where M = Pd and Pt) complexes. For some of these compounds, structure determination revealed structural distortions suggesting weak intramolecular Cl–Sb interactions, which were confirmed by theoretical methods.

Introduction

Stibine ligands have long been overlooked in favour of the ubiquitous phosphines.[1] This situation was possibly influenced by the simplified notion that stibines are simple phosphine analogues, albeit less stable (due to the weaker Sb–C bonds) and weaker coordinating ligands. Although many parallels can be found between the chemistries of phosphine and stibine ligands, stibines exhibit additional peculiar features that make them attractive, such as changed stereochemical profiles (typically lower steric demands than for the corresponding phosphines), increased Lewis acidity, and facile conversion into Lewis acidic stiboranes.[2] In the chemistry of ferrocene ligands,[3] compounds bearing stibine substituents were long limited to (diphenylstibino)ferrocene derivatives bearing donor groups at position 2 of the ferrocene scaffold, which were studied for possible Sb-donor interactions.[4,5]

Recently, we synthesised 1,1′-bis(diphenylstibino)ferrocene (**1** in Scheme 1),[6] which is a direct analogue of the widely studied 1,1′-bis(diphenyphosphino)ferrocene (dppf),[7] and explored the reactivity and coordination behaviour of this compound.[6] In the following research, we focused on the analogous mixed-donor derivative 1-(diphenylphoshino)-1′-(diphenylstibino)ferrocene (**2**) and its P(v)- and Sb(v)-derivates.[8] These compounds were studied mainly because of possible intramolecular dative interactions between the P- and Sb-substituents,

Department of Inorganic Chemistry, Faculty of Science, Charles University, Hlavova 2030, Prague 128 40, Czech Republic. E-mail: stepnic@natur.cuni.cz

† Electronic supplementary information (ESI) available: Complete experimental details, additional structure diagrams, result from the DFT calculations, additional cyclic voltammograms, copies of the NMR spectra and Cartesian coordinates for the DFT-optimised structures. CCDC 2320741–2320757. For ESI and crystallographic data in CIF or other electronic format see DOI: https://doi.org/10.1039/d4nj00349g

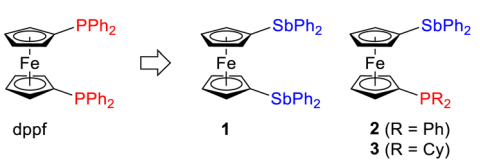

Scheme 1 Structures of dppf and compounds **1**–**3** (Cy = cyclohexyl).

which were indeed identified in stiboranes resulting from oxidation of the stibine moiety. Unfortunately, studies on the coordination behaviour of **2** were hampered by the tendency of this compound to form disordered structures, in which the phosphine and stibine groups alternated in their positions.

To circumvent this problem, we synthesised desymmetrised derivative **3** bearing cyclohexyl (Cy) substituents at the phosphorus atom. This compound allowed us to not only study the coordination properties of this hybrid P,Sb-ligand but also elucidate the influence of the phosphine substituents on the interactions between the functional groups in **3** and its oxidised derivatives. In particular, we report here the synthesis of **3** and analogous compounds with P(v) or Sb(v) substituents, detailed experimental and theoretical characterisation of these compounds focused on interactions between the pnictogen substituents and a study of the coordination behaviour of **3** as a new, hybrid P,Sb-ligand.[9]

Results and discussion

Preparation and reactivity of compound 3

Phosphinostibine **3** was obtained by sequential lithiation/functionalisation of 1,1′-dibromoferrocene[10,11] (Scheme 2) and was isolated as an air-stable orange solid in approximately 40% yield over the two reaction steps after final crystallisation. Attempted synthesis of **3** using a ''one-pot'' approach (*i.e.*, without isolation of intermediate **4**) proved unsuitable because the isolated crude product contained substantial amounts of monosubstituted side products $FcSbPh_2$ and $FcPCy_2$ (Fc = ferrocenyl), which could not be efficiently removed by chromatography and crystallisation.

To illustrate the different reactivities of the two pnictogen substituents, compound **3** was treated with elemental sulfur (1 equiv.) and $BH_3{\cdot}SMe_2$ (1.5 equiv.). Under such conditions, only the phosphine moiety reacted to give phosphine sulfide **3S** and adduct **3**·BH_3. Synthesis of the corresponding phosphine oxide **3O** could not be similarly performed (*e.g.*, with H_2O_2 as the usual oxidant) because of unwanted reactions at the stibine moiety. Alternatively, this compound was obtained similarly to **3** through lithiation of precursor **4O**, which had a preinstalled phosphine oxide moiety, followed by subsequent reaction with $ClSbPh_2$. The reaction between **3** and [AuCl(tht)] (1 equiv., tht = tetrahydrothiophene) afforded a phosphine complex [AuCl(**3**-κP)] (**5**) as the sole product, in line with our previous observations.[8]

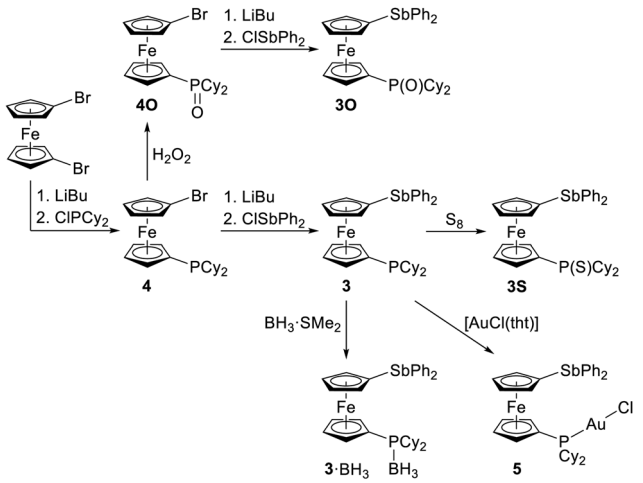

Scheme 2 Synthesis of **3** and further modifications to the phosphine moiety (Cy = cyclohexyl, tht = tetrahydrothiophene)

Table 1 Comparison of the ^{31}P NMR shifts[a]

Compound	**3E/5**	**6E/7**	**8E/10**
E = void	−7.5	—[b]	2.2
E = BH_3	24.3	24.5	24.3
E = O	45.9	—[b]	53.8[c]
E = S	57.5	57.1	57.0
Au(I) complex	42.3	41.0	41.1

[a] The $^{31}P\{^1H\}$ NMR spectra were recorded in $CDCl_3$ at 25 °C unless otherwise indicated. [b] Compound was not prepared. [c] In CD_2Cl_2.

All the compounds were characterised by a combination of multinuclear NMR spectroscopy, electrospray ionisation (ESI) mass spectrometry, and elemental analysis, and in most cases, the solid-state structures were established by single-crystal X-ray diffraction analysis. The NMR spectra showed signals of the asymmetrically 1,1′-disubstituted ferrocene unit and characteristic signals of the cyclohexyl[12] and phenyl substituents at the pnictogen groups (especially in the $^{13}C\{^1H\}$ NMR spectra). The manipulation of the phosphine substituent was reflected in the $^{31}P\{^1H\}$ NMR spectra (Table 1). Of particular note are the similarities in the ^{31}P NMR shifts determined for **3E** (E = void, BH_3, O, and S) and **5** to those for analogous ''simple'' compounds such as (dicyclohexylphosphino)ferrocene (δ_P −6.0) and its *P*-oxide (δ_P 46.8),[13] 1,1′-bis(dicyclohexylphosphinothioyl)ferrocene ($fc(P(S)Cy_2)_2$; fc = ferrocene-1,1′-diyl,[14] δ_P 57.3), 1-(dicyclohexylphosphino)-1′-methylferrocene–borane (1 : 1) ($Cy_2PfcMe{\cdot}BH_3$; δ_P 24.1),[15] and the complex [{μ(P,P′)-$fc(PCy_2)_2$}$(AuCl)_2$] (δ_P 41.2; all values in $CDCl_3$),[16] which ruled out any significant interactions between the stibine moiety and the phosphorus substituents in all cases.

The molecular structures of **3**, **3**·BH_3, **3O**, and **3S** (Fig. 1 and Table 2) were generally similar. The ferrocene units adopted their usual geometry with practically negligible tilting of the cyclopentadienyl rings (<5°) and similar open 1,3′ conformations[17] (*cf.* the τ angles with the ideal value of 144°). Even the substituents at the pnictogen atoms were similarly positioned, with one pointing away from the ferrocene unit and one directed to the side. The Sb–C bonds (Sb–C(fc) < Sb–C(Ph)) varied rather marginally in the entire series in contrast to the P–C bonds, which were affected by transformations of the phosphine moiety. Specifically, the introduction of the fourth substituent to the phosphorus atom resulted in a decrease in the P–C distance (more in the P-chalcogenides **3O** and **3S** than in **3**·BH_3). A similar trend could be found for tricyclohexylphosphine and its derivatives, which also had comparable P–E bond lengths.[18] The C–Sb–C angles were smaller[19] than the C–P–C angles, which further opened upon addition of the

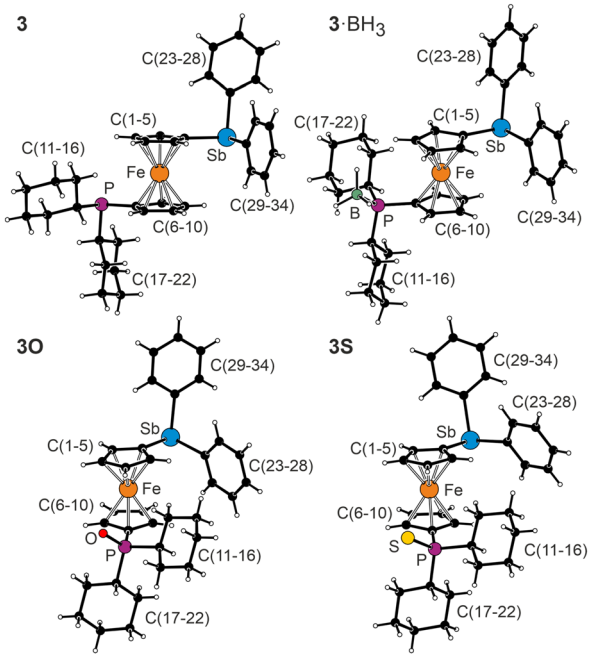

Fig. 1 Molecular structures of **3**, **3**·BH_3, **3O** and **3S** (for displacement ellipsoid plots, see the ESI†).

Table 2 Selected distances and angles for **3**, **3**·BH_3, **3O** and **3S** (in Å and deg)

Parameter[a]	3	3·BH_3	3O	3S
E	Void	B	O	S
Sb–C1	2.125(3)	2.131(2)	2.150(2)	2.129(2)
Sb–C23	2.146(3)	2.153(2)	2.156(2)	2.155(2)
Sb–C29	2.160(4)	2.157(3)	2.160(2)	2.154(2)
P–C6	1.828(3)	1.800(2)	1.787(2)	1.793(1)
P–C11	1.856(3)	1.839(2)	1.824(2)	1.834(1)
P–C17	1.868(3)	1.839(3)	1.821(2)	1.842(1)
∠Cp1,Cp2	2.8(2)	1.7(1)	3.61(9)	3.15(8)
τ	−139.9(2)	−141.7(2)	−142.6(1)	−137.6(1)
P–E	—[b]	1.932(3)	1.491(1)	1.9635(5)

[a] Definitions: Cp1 and Cp2 are the cyclopentadienyl rings C(1–5) and C(6–10), respectively, and Cg1 and Cg2 represent their centroids. τ is the torsion angle C1–Cg1–Cg2–C6. [b] Not applicable.

fourth substituent. All cyclohexyl rings adopted a chair conformation with the ring puckering parameter θ[20] deviating by no more than 3° from the ideal value of 0/180° in the entire series, and the pivotal P–C bonds occupied equatorial positions.

Notably, the individual molecules of **3O** assembled into chains *via* non-bonding contacts between the stibine Sb and phosphoryl oxygen from adjacent molecule (Sb···O = 3.033(1) Å; Fig. S3, ESI†). No such interactions were observed in the structures of **3** and **3S**.

Further experiments focused on compounds oxidised at the stibine moiety, namely, on stiboranes. Unfortunately, direct oxidation of **3** with thionyl chloride or sulfuryl chloride failed to provide the targeted phosphino-stiborane due to the concurrent oxidation of the phosphine moiety. Reaction of **3** with $SOCl_2$ produced the doubly oxidised product $Cy_2P(S)fcSbCl_2Ph_2$

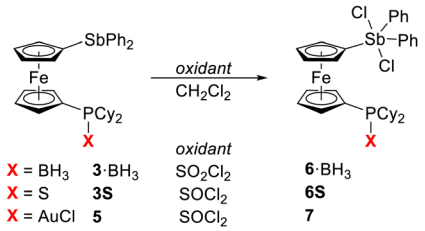

Scheme 3 Oxidation of **3O**, **3**·BH_3 and Au(I) complex **5**.

(**6S**; 56% in the reaction mixture), which arose from unwanted thionation of the phosphine moiety with *in situ* generated sulfur,[21] and two additional unidentified products. The analogous reaction employing SO_2Cl_2 resulted in a mixture of several products dominated by an unidentified species showing a broad ^{31}P NMR resonance at δ_P 67.6 (≈84%).

Conversely, oxidation of **3**·BH_3 and **3S**, whose phosphine moieties were efficiently protected, smoothly proceeded, producing the respective dichlorostiboranes **6**·BH_3 and **6S** (Scheme 3). Even so, oxidation of Au(I) complex **5** afforded an analogous complex with a "terminal" stiborane substituent, [AuCl(Cy_2Pfc-$SbCl_2Ph_2$-κP)] (**7**), in nearly quantitative yield (96%, Scheme 3). Notably, while oxidation of **3S** and **5** could be achieved equally well with $SOCl_2$ and SO_2Cl_2, oxidation of **3**·BH_3 had to be performed with $SOCl_2$ because a similar reaction of **3**·BH_3 with SO_2Cl_2 as the halogenating agent produced **6**·BH_3 contaminated by ≈25% of another compound giving rise to a ^{31}P NMR signal at δ_P 8.4. The side product, presumably the boron-halogenated compound **6**·BH_2Cl,[22] could not be simply separated because all dichlorostiboranes readily decomposed on silica gel (most likely *via* hydrolysis at the column) and had to be purified by crystallisation, which proved inefficient for this particular mixture.

Compounds **6**·BH_3, **6S** and **7** were characterised similarly to their precursors. Oxidation of the stibine moiety was mainly reflected in the ^{13}C NMR spectra, which showed that the signals due to Sb-bound aromatic rings (C_5H_4 and Ph) shifted to a lower field than those of the respective precursor. In contrast, the ^{31}P NMR shifts (Table 1) only slightly differed from those of the stibine analogues, confirming the absence of any significant Sb–S interactions in **3S**, which is indeed in line with the results of crystal structure determination (Fig. 2 and Table 3).

While the transformation of the stibine moiety left the PCy_2·BH_3 moiety and conformation of the ferrocene unit in the structure of **6**·BH_3 virtually unchanged, the arrangement around the Sb atom was changed to trigonal bipyramidal with the Cl atoms located at axial positions (Cl1–Sb–Cl2 177.25(2)°), and the Sb–C bonds were shortened by ≈0.04 Å (compared to **3**·BH_3). The τ_5 index[23] (0.91) indicated only a minor distortion (the ideal trigonal bipyramid would yield τ_5 = 1.00), likely due to variations in the equatorial angles (C–Sb–C = 116.45(6)–122.47(6)°).

Similar features were observed in the structure of **6S**, where one of the phenyl rings was partly disordered, and complex **7**, which crystallised with two independent molecules per asymmetric unit (one molecule showed disorder of the phenyl rings;

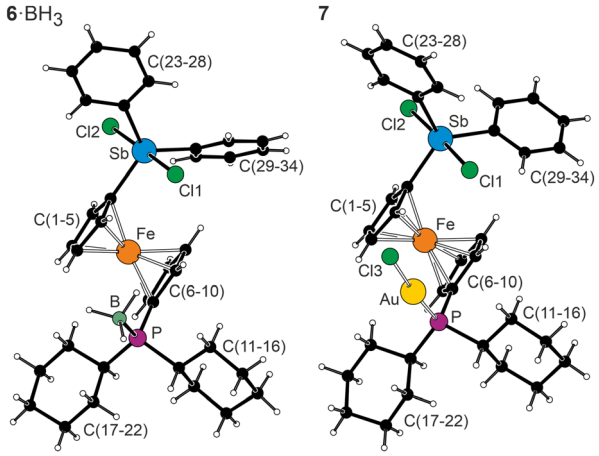

Fig. 2 Structures of **6**·BH_3 and **7** (molecule 1). Additional structure diagrams (including that of **6S**, which is isostructural with **6**·BH_3) are available in the ESI.†

Table 3 Selected distances and angles for **6**·BH_3, **6S** and **7** (in Å and deg)

Parameter[a]	**6**·BH_3	**6S**	**7** (mol 1)	**7** (mol 2)
E	B	S	Au	Au
Sb–C1	2.083(1)	2.078(2)	2.094(6)	2.090(6)
Sb–C23	2.104(2)	—[b]	2.123(5)	—[b]
Sb–C29	2.122(2)	2.121(2)	2.137(6)	—[b]
Sb–Cl1	2.4586(4)	2.4721(5)	2.442(1)	2.462(2)
Sb–Cl2	2.4651(4)	2.4540(5)	2.476(1)	2.462(2)
P–C6	1.805(1)	1.802(2)	1.806(6)	1.805(5)
P–C11	1.839(2)	1.837(2)	1.840(5)	1.835(5)
P–C17	1.839(1)	1.840(2)	1.841(6)	1.832(5)
∠Cp1,Cp2	3.35(9)	3.3(1)	1.5(4)	3.5(3)
τ	141.5(1)	−141.7(2)	124.8(4)	−152.8(4)
P–E	1.940(2)	1.9642(6)	2.229(1)	2.237(1)

[a] The parameters are defined similarly as for the parent stibines (see footnote to Table 1). [b] Value affected by disorder.

in this case, the conformation of the ferrocene unit differed between the two molecules). The P–Au–Cl units in **7** were linear (molecule 1/2: 175.29(6)/177.32(5)°), and the interatomic distances therein (Au–P 2.229(1)/2.237(1) Å, Au–Cl 2.298(1)/2.299(2) Å) were comparable to the values determined for [AuCl(Cy$_2$PfcCN-κP)] (Au–P 2.2319(7) Å, Au–Cl 2.2850(7) Å).[24]

Synthesis and structural characterisation of catecholatostiboranes

To further enhance the Lewis acidity of the antimony atom and thus elicit possible dative P/P=E → Sb interactions, additional Sb(v) derivatives were prepared *via* oxidation of compounds with free stibine groups with *o*-chloranil (3,4,5,6-tetrachloro-1,2-benzoquinone). Even in this case, direct oxidation of free phosphine **3** was rather difficult due to the poor selectivity[25] (Scheme 4). The reaction of **3** with 1 equiv. *o*-chloranil produced a mixture containing unreacted **3**, the targeted stiborane **8**, and the corresponding phosphine oxide **8O** in an approximately 3 : 3 : 4 ratio. This suggested that both stibine and phosphine moieties were oxidised with *o*-chloranil but that the

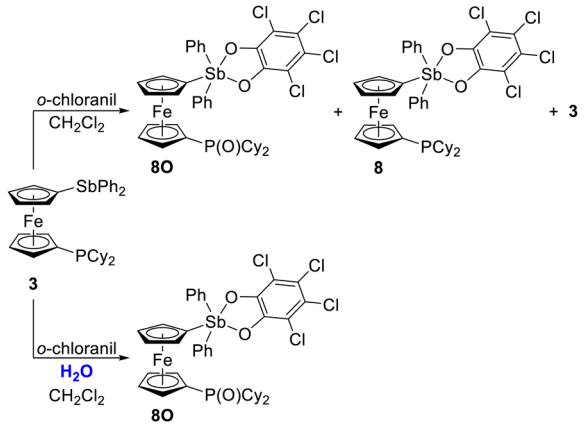

Scheme 4 Oxidation of **3** with *o*-chloranil.

phosphorane was hydrolysed more easily to give phosphine oxide **8O**.[8] Indeed, a reaction performed using dried reagents allowed isolation of the unstable intermediate Cy$_2$P(O$_2$C$_6$Cl$_4$)fc-SbPh$_2$(O$_2$C$_6$Cl$_4$) (**9**), which cleanly converted into **8O** when treated with water. When water was present in the reaction mixture (introduced as a wet solvent), oxidation of **3** produced **8O** as the sole product in good yield (85%).

Oxidation of adduct **3**·BH_3, phosphine chalcogenides **3O** and **3S**, and model Au(I) complex **6** proceeded without any complications and afforded corresponding stiboranes **8**·BH_3, **8O**, **8S**, and **10** in good yields after crystallisation (Scheme 5). This ultimately enabled an alternative route towards **8** based on deprotection[26] of borane adduct **8**·BH_3 with 1,4-diazabicyclo[2.2.2]octane (dabco) in warm THF (Scheme 5) to be devised, which avoided problems associated with product isolation (the compounds decomposed on silica gel, which substantially complicated isolation of individual products from their mixtures, *e.g.*, when **8** and **8O** were both present).

Initial NMR characterisation of the catecholatostiboranes already indicated differences between compounds **8**/**8O** and **8**·BH_3/**8S**/**10**. While the $^{31}P\{^1H\}$ NMR signals of the latter compounds were observed at positions similar to those of the signals of the respective precursors (*i.e.*, **3**·BH_3, **3S** and **5**), the $^{31}P\{^1H\}$ NMR signals of **8** and **8O** significantly shifted to a lower field (Table 1), thus suggesting the presence of P → Sb and O → Sb interactions. For **8**, the dative interaction was further indicated by splitting of the signals due to C^{ipso} carbons in the Sb-bound C_5H_4 and Ph rings into ^{31}P-coupled doublets (even one of the cyclopentadienyl CH groups showed such

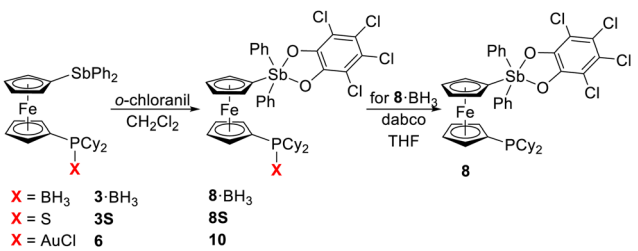

Scheme 5 Synthesis of catecholatostiboranes.

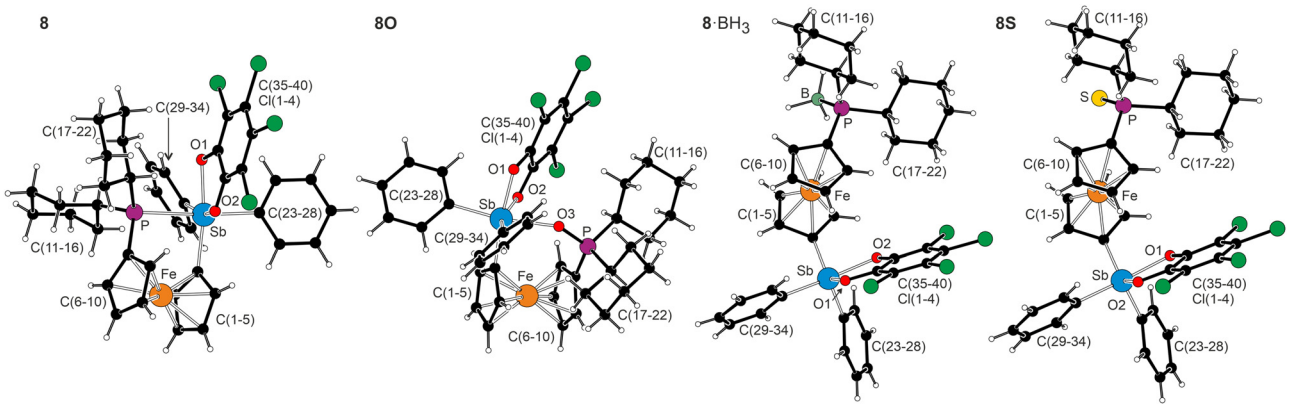

Fig. 3 Molecular structures of **8**·C_6H_{14} (molecule 1), **8O** (molecule 1), **8**·BH_3 and **8S** (complete structure diagrams are available in the ESI†).

interactions), which was not observed in the $^{13}C\{^1H\}$ NMR spectra of the other compounds.

No similar interactions were obviously possible in the compounds where the phosphorus substituent was "blocked" by the formation of a Lewis adduct and coordination (**8**·BH_3 and **10**) and was not even suggested for phosphine sulfide **8S.** This trend was clearly manifested in the crystal structures of **8**, **8O**, **8S** and **8**·BH_3 (Fig. 3 and Table 4).

The crystal structure of solvated **8** contained two practically identical, albeit crystallographically independent, stiborane molecules (Fig. S23, ESI†), whose arrangement implied a strong P–Sb interaction. The P–Sb separation (≈2.81 and 2.83 Å in the two molecules) was shorter than that in the analogous compound with phenyl substituents, $Ph_2PfcSbPh_2(O_2C_6Cl_4)$ (**8Ph**, 3.0987(6) Å), in line with the occurrence of an interaction enhanced by the increased electron-donating ability of the phosphine group (*N.B.* the P–Sb distance falls between the sum of the covalent radii and the sum of the van der Waals radii, 2.46 and 3.86 Å,[27] being closer to the former). The phosphorus atom thus completed an octahedral coordination sphere around the Sb atom, where the interligand *cis*-angles ranged from approximately 78–104° (in both molecules), with the smallest angle associated with the catecholate ligand (O1–Sb–O2) and the widest angle for C1–Sb–C29 at the adjacent position. The Sb atom was displaced from the "equatorial" plane defined by C1, C29, O1 and O2 towards C23 by approximately 0.2 Å, and the P–Sb–C23 axis was slightly bent (169.97(1)/170.2(1)° in molecule 1/2). Compared to the structure of the parent stibine **3**, the ferrocene substituents in **8** were rotated closer, allowing for the P–Sb interaction (*cf.* τ angles in Tables 2 and 3).

The structure of **8O** was generally similar except that the P═O···Sb distances were more similar to the values reported for $Ph_2P(O)fcSbPh_2(O_2C_6Cl_4)$ (2.256(1) Å; *N.B.* the influence of the phosphine substituents was now only indirect). The interligand angles within the octahedron surrounding the Sb atoms were approximately 77–106°, with the largest value occurring for the C23–Sb–C29 angle (*cf.* O–Sb–C23 = 168.18(8)/171.48(9)°). By featuring a longer "bridge" between the cyclopentadienyl rings, the ferrocene units in **8O** exhibited more relaxed conformations (with larger τ) and lower tilt angles.

Compounds **8**·BH_3 and **8S** crystallised isostructurally and their molecules adopted extended structures with substituents at the ferrocene unit in remote positions (the τ values were similar to those of **3**·BH_3 and **3S**). While the arrangements of the phosphorus substituents in **8**·BH_3 and **8S** were similar to those in the respective parent compounds, the ψ-tetrahedral stibine groups were converted into pentacoordinate stiborane

Table 4 Selected distances and angles for **8**·C_6H_{14}, **8O**, **8**·BH_3 and **8S** (in Å and deg)

Parameter[a]	**8**·C_6H_{14} (molecule 1)	**8**·C_6H_{14} (molecule 2)	**8O** (molecule 1)	**8O** (molecule 2)	**8**·BH_3	**8S**
E	Void	Void	O	O	B	S
P/E···Sb	2.8126(9)	2.8288(9)	2.255(2)	2.187(2)	n.a.	n.a.
Sb–C1	2.146(3)	2.127(3)	2.113(3)	2.117(3)	2.079(2)	2.073(2)
Sb–C23	2.132(3)	2.134(4)	2.142(3)	2.150(3)	2.099(2)	2.097(2)
Sb–C29	2.134(3)	2.142(3)	2.132(2)	2.143(3)	2.137(2)	2.135(2)
Sb–O1	2.084(2)	2.081(2)	2.079(2)	2.076(2)	2.020(1)	2.111(2)
Sb–O2	2.122(2)	2.119(3)	2.075(2)	2.089(2)	2.110(1)	2.016(1)
P–C6	1.806(3)	1.798(4)	1.795(3)	1.779(3)	1.805(2)	1.806(2)
P–C11	1.844(3)	1.847(3)	1.811(3)	1.808(4)	1.844(2)	1.838(2)
P–C17	1.857(3)	1.852(3)	1.821(3)	—[b]	1.843(2)	1.837(2)
∠Cp1,Cp2	5.7(2)	4.8(2)	3.2(2)	1.3(2)	2.23(9)	2.2(1)
τ	17.9(2)	−16.4(2)	22.4(2)	−28.2(2)	142.8(1)	143.4(1)
P–E	n.a.	n.a.	1.519(2)	1.519(2)	1.927(2)	1.9562(7)

[a] The parameters are defined the same as those for the parent stibines (see footnote to Table 1). n.a. = not applicable. [b] Parameter affected by disorder of the phenyl ring.

moieties with a severely distorted arrangement, as indicated by the τ_5 indices (τ_5 = 0.55 for **8**·BH_3 and 0.56 for **8S**), which were practically halfway between the values expected for an ideal trigonal bipyramid (1.0) and an ideal square pyramid (0.0).[23] However, the bond distances did not significantly differ from those determined for $Ph_3Sb(O_2C_6Cl_4)$.[28]

Analysis of the bonding situation and electrochemistry

The nature and strength of the intramolecular interactions in stiboranes **8** and **8O** were evaluated through topological analysis of the electron density using the Atoms in Molecules (AIM) theory[29] (Fig. 4). Compound **8S**, for which no P=S → Sb interaction was detected, was included in the calculations for comparison.

The experimentally proven presence or absence of intramolecular interactions already matched the calculated energy differences between the (hypothetical) "open" and "closed" forms of the investigated species (Table 5). While the closed (interacting) forms of stiboranes **8** and **8O** were strongly favoured in both vacuum and chloroform (the solvent effects were approximated by the PCM model[30]), the difference in energy between the open and closed forms of **8S** was practically negligible, and the former arrangement was even slightly preferred when solvent effects were considered.

Table 5 Free energy differences (in kJ mol^{-1} at 298.15 K) between the different stereoisomers of stiboranes **8**, **8O**, and **8S**[a]

Compound	Vacuum	Chloroform
8	−27	−29
8O	−47	−41
8S	−3	+0.4

[a] Calculated at the PBE0(d3)/def2-TZVP:sdd(Fe,Sb) level of theory. Solvent effects were approximated using the PCM model (see Experimental section).

The values of the calculated real space functions (Table 6) were mostly in agreement with the values recently reported[8] for

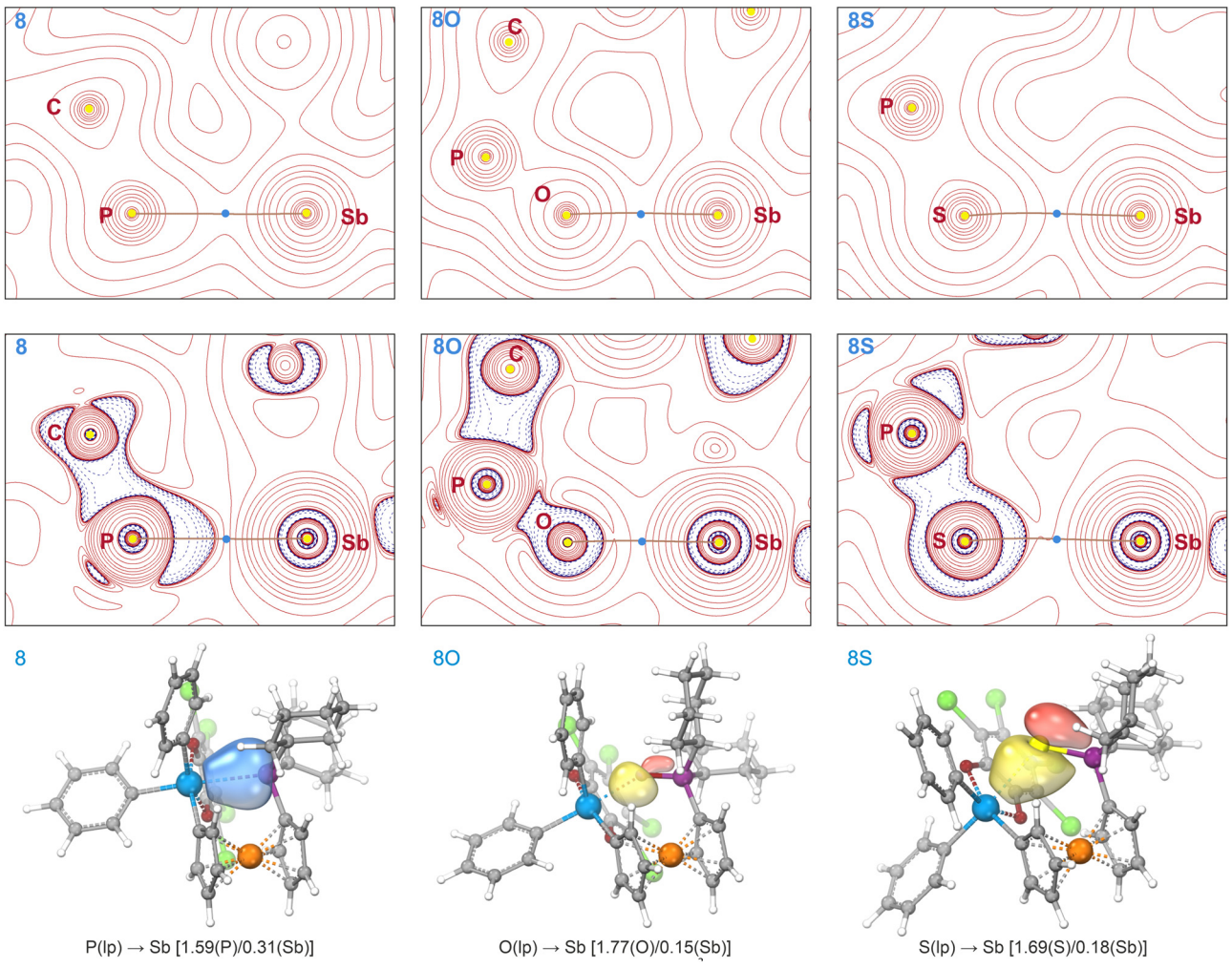

Fig. 4 Contour plots of the electron density ρ (top) and Laplacian of the electron density $\nabla^2\rho$ (middle; positive – full red lines, negative – dashed blue lines) in the plane defined by the pivotal C, P and Sb (for **8**) or by chalcogen atoms (O or S), P and Sb (for **8O** and **8S**). The yellow and blue dots indicate the positions of the critical points, and the brown lines indicate the P–Sb and E–Sb bond paths. (bottom) Selected intrinsic bond orbitals (IBOs) of stiboranes **8**, **8O** and **8S**. The values in parentheses indicate the fraction of bonding electrons assigned to the individual atoms (lp = lone pair).

Table 6 Values of the electron density (ρ_{bcp}), electron density Laplacian ($\nabla^2\rho_{bcp}$), total energy density (H_{bcp}), ratio of the potential to the kinetic energy density ($|V_{bcp}|/G_{bcp}$), and ratios of the kinetic (G/ρ_{bcp}) and total energy (H/ρ_{bcp}) densities to the electron density at the bond critical point located between the antimony atom and a donor atom, as well as the corresponding bond distances (experimental and calculated)[a]

Compd	Bond	Bond length [Å]		ρ_{bcp} [e Å^{-3}]	$\nabla^2\rho_{bcp}$ [e Å^{-5}]	H_{bcp} [a.u.]	$\lvert V_{bcp}\rvert/G_{bcp}$ [a.u.]	G_{bcp}/ρ_{bcp} [a.u.]	H_{bcp}/ρ_{bcp} [a.u.]
		Experimental	Calculated						
8	P···Sb	2.8126(9)/2.8288(9)	2.859	0.047	0.026	-1.17×10^{-2}	2.10	0.22	−0.25
8O	O···Sb	2.255(2)/2.187(2)	2.298	0.054	0.170	-1.20×10^{-2}	1.44	0.51	−0.22
8S[b]	S···Sb	—[c]	2.898	0.035	0.044	-0.60×10^{-2}	1.51	0.34	−0.17

[a] Calculated at the PBE0(d3)/def2-TZVP:sdd(Sb,Fe) level of theory. [b] Hypothetical closed isomer. [c] Not available.

analogous stiboranes bearing only phenyl substituents (*i.e.*, compounds derived from phosphinostibine **2**). The low electron densities (ρ_{bcp}) and positive values for their Laplacians ($\nabla^2\rho_{bcp}$) at the bond critical points (bcps) corresponded to values typical for donor–acceptor "complexes" involving heavy elements with diffuse valence shells (such as antimony).[31] A closer inspection of the calculated local properties revealed that the values previously found for stiboranes $Ph_2P(E)fcSbPh_2(O_2C_6Cl_4)$ (E = O or S) were practically identical to those estimated for chalcogenides **8O** and **8S** described here. However, significant differences were noted for $Ph_2PfcSbPh_2(O_2C_6Cl_4)$ (**8Ph**) and **8**. The most significant difference was the change in the ratio of the potential to the kinetic energy density ($|V_{bcp}|/G_{bcp}$) at the bcps. The magnitude of this parameter indicates whether the bonding has a prevalently covalent ($|V_{bcp}|/G_{bcp} > 2$) or ionic ($|V_{bcp}|/G_{bcp} < 1$) character,[32] while values falling in the intermediate region ($2 > |V_{bcp}|/G_{bcp} > 1$) are characteristic of dative interactions, as in the case of all chalcogenide derivatives $R_2P(E)fcSbPh_2(O_2C_6Cl_4)$ (R = Cy and Ph) and phenyl-substituted phosphinostiborane **8Ph** previously studied.

In addition, the value calculated for **8** ($|V_{bcp}|/G_{bcp}$ = 2.10) suggested an increase in the covalent character of the P → Sb dative interaction in this compound. The increased covalent nature was further implied by the higher energy density at the bcp and by the more negative total energy density-to-electron density ratio, H_{bcp}/ρ_{bcp}. An inspection of the Laplacian profiles along the P → Sb bond path in **8** and **8Ph** (see the ESI,† Fig. S24) revealed a slightly greater accumulated charge density in the region of the phosphorus lone electron pair for **8**. In addition, the corresponding valence shell charge concentration (VSCC) was shifted closer to the bcp, which otherwise lies in the charge-depleted region. The higher covalency of the P → Sb interaction in **8** compared to that in its phenyl analogue **8Ph** was also indicated by the calculated Mayer bond orders (MBOs: 0.56 in **8** and 0.49 in **8Ph**) and Wiberg bond indices (WBIs: 0.30 and 0.22, respectively). In contrast, the low values of both the MBO and WBI (Table 7) found for **8O** implicated that the electrostatic contribution was the dominant component of the P═O → Sb interaction, as also reflected by the relatively high value of the kinetic energy density-to-electron density ratio G_{bcp}/ρ_{bcp}. This indeed corresponded with the higher polarisation of the P═O bond towards $P^{(+)}$–$O^{(-)}$.[33]

The conclusions obtained from the topological analysis were further supported by intrinsic bond orbital (IBO) analysis.[34] The IBOs corresponding to the interaction between the antimony and respective donor atoms are also shown in Fig. 4. The charge distribution between bonded atoms reflects the different degrees of electron sharing (for an ideal covalent bond, it would be exactly 1.0/1.0). The greater charge localisation at the acceptor atom indicated higher covalency of the P → Sb interaction in **8** [P(1.59)/Sb(0.31)] compared not only to its chalcogenide derivatives **8O** [O(1.77)/Sb(0.15)] and **8S** [S(1.69)/Sb(0.18)] but also to the cognate compound **8Ph** [P(1.68)/Sb(0.20)]. This increase reflected an increase in the donation ability of the phosphine group upon introduction of cyclohexyl substituents, which was also suggested by the substantially higher methyl cation affinity (MCAs)[35] estimated for the phosphine group in **3** (P: 695, Sb: 552 kJ mol^{-1}) as compared to the phenyl analogue **2** (P: 549, Sb: 675 kJ mol^{-1};[8] calculated at the PBE0(d3)/def2-TZVP:sdd(Fe,Sb) level of theory in vacuum).

Table 7 Selected Mayer bond orders (MBOs) and Wiberg bond indices (WBIs) for **8**, **8O** and **8S** (closed isomers)[a]

Compound	MBO		WBI	
	P/E···Sb	P═E	P/E···Sb	P═E
8	0.56	n.a.	0.30	n.a.
8O	0.07	1.27	0.19	2.05
8S	0.55	1.36	0.24	1.80

[a] Calculated at the PBE0(d3)/def2-TZVP:sdd(Sb,Fe) level of theory. n.a. = not applicable.

Considering that all the compounds contain the redox-active ferrocene unit, whose redox potential reflects the electronic influence of the substituents and can thus be used as a reporter group at the molecular level, stibines **3**, **3**·BH_3, **3O** and **3S** and the corresponding catecholatostiboranes were studied by cyclic voltammetry on a glassy carbon disc electrode in CH_2Cl_2 containing $Bu_4N[PF_6]$ as a supporting electrolyte. Attention was given to the primary electrochemical oxidations, which were assumed to occur at the ferrocene unit. For **3** and **3O** as the model compounds, this was supported by DFT calculations showing that the highest occupied molecular orbitals (HOMOs) were localised predominantly at the ferrocene unit, though with a significant contribution from the phosphorus orbitals for phosphine **3**. Conversely, the HOMOs of stiboranes **8** and **8O** were localised mainly at the tetrachlorocatecholate units (see the ESI,† Fig. S25).

The initial oxidation of the phosphine chalcogenides and borane adducts (Fig. 5 and Fig. S28–S30, ESI†) was reversible, even though additional irreversible redox transitions could be

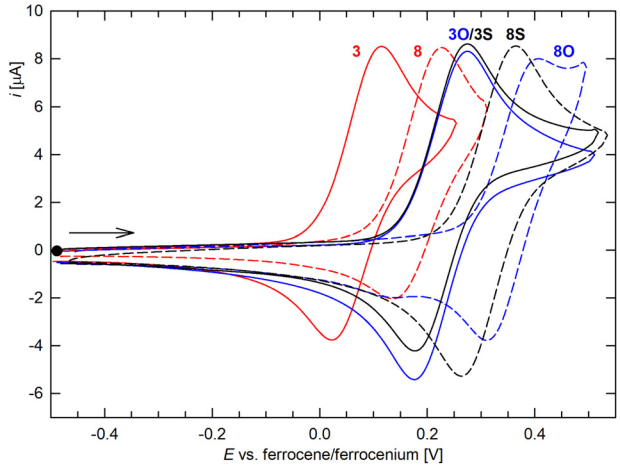

Fig. 5 Cyclic voltammograms for **3**, **3O** and **3S** and the corresponding stiboranes **8**, **8O** and **8S**, showing the first oxidative wave (glassy carbon disc electrode, 0.1 M $Bu_4N[PF_6]$ in CH_2Cl_2, scan rate 100 mV s^{-1}).

detected at more positive potentials for most compounds (these redox changes were not investigated further). In contrast, the oxidation of **3** and **8** was only quasireversible, appearing virtually reversible at relatively fast scan rates (100 mV s^{-1} or higher) but losing reversibility when the scan rate was decreased, most likely due to associated chemical reactions that consumed the electrogenerated species, as is typical for (uncoordinated) ferrocene phosphines (*cf.* the HOMO).[36]

The redox potentials of the first oxidation were 0.06 V for **3**, 0.23 V for **3**·BH_3, 0.22 V for **3O**, and 0.23 V for **3S** relative to the ferrocene/ferrocenium (ref. 37). This trend roughly corresponded with the electronic nature of the substituents, as suggested by the Hammett σ_p constants (0.19 for PPh_2, 0.53 for $P(O)Ph_2$, and 0.47 for $P(S)Ph_2$).[38,39]

Oxidation of the stibine moiety resulted in a shift towards more positive potentials ($E^{\circ\prime}$ = 0.18 V for **8**, 0.30 V for **8**·BH_3, 0.36 V for **8O**, and 0.32 V for **8S**), which indicated that the electron density at the ferrocene unit decreased. Notably, the differences in the stibine-stiborane pairs were substantially smaller for the borane adducts and phosphine sulfides, for which no interactions were detected between the P- and Sb-substituents (ΔE = 0.07 and 0.08 V), than for the compounds showing dative P → Sb and O → Sb interactions (ΔE = 0.12 and 0.14 V). This could be tentatively ascribed to the intramolecular interactions reducing the electron density at the P-substituents, thereby decreasing the ability of the phosphorus groups to buffer the decrease in electron density associated with stibine-to-stiborane conversion.

Coordination study with phosphinostibine 3

One of the original aims of the present work was to study the coordination behaviour of **3** towards selected metals. For this purpose, we chose soft, late transition metal ions with different coordination geometries. As stated above, compound **3** reacted with 1 molar equiv. of [AuCl(tht)] to produce [AuCl(**3**-κP)] (**5**), in which only the more basic phosphine group coordinated

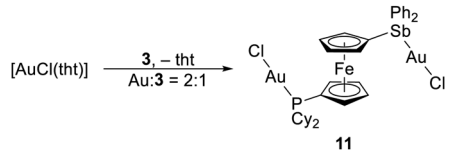

Scheme 6 Preparation of complex **11** (tht = tetrahydrothiophene).

(*vide supra*). A similar behaviour was reported for **2**,[8] while **1** produced the ionic, ligand-redistribution product $[Au(\mathbf{1}\text{-}\kappa^2Sb,Sb')_2][AuCl_2]$,[6] and dppf gave rise to the coordination polymer $[AuCl(dppf)_n]$[40] or polynuclear species[41] under similar conditions. In contrast, the reaction between **3** and 2 equiv. of the Au(I) precursor (Scheme 6) afforded the symmetrical, ligand-bridged digold complex $[(\mu(P,Sb)\text{-}\mathbf{3})(AuCl)_2]$ (**11**; δ_P 40.7), similar to compounds resulting from dppf,[42] **1** and **2**.

The salient feature of the solid-state structure of **11** (Fig. 6) was the intramolecular aurophilic interaction[43] (Au···Au = 3.1371(4) Å, Cl–Au–Au–Cl = −101.69(2)°) between the linear LAuCl units, which controlled the conformation of the ferrocene unit (τ = −79.4(1)°, tilt angle: 5.0(1)°). A similar arrangement was noted in $[(\mu(Sb,Sb')\text{-}\mathbf{1})(AuCl)_2]$ (Au···Au = 2.9878(5) Å) but not in either the polymorphs or solvatomorphs of the analogous dppf complex.[42,44] Parameters pertaining to the individual "LAuCl" moieties were unexceptional in view of those reported for $[AuCl(FcSbPh_2\text{-}\kappa Sb)]$[8] and $[AuCl(Cy_2PfcCN\text{-}\kappa P)]$.[24]

Reaction of **1** with $[RuCl(\mu\text{-}Cl)(\eta^6\text{-}p\text{-cymene})]_2$ (Ru : **3** = 2 : 1) in dichloromethane produced a mixture of the anticipated bridged complex $[(\mu(P,Sb)\text{-}\mathbf{3})\{RuCl_2(\eta^6\text{-}p\text{-cymene})\}_2]$ (≈95%; δ_P 18.4) and a minor unidentified species (≈5%; δ_P 17.6). Unfortunately, repeated attempts to isolate the bridged complex failed due to decomposition of the reaction mixture upon crystallisation or prolonged standing. A product mixture was also obtained when the ligand amount was reduced to one molar equivalent per Ru. Gratifyingly, addition of $Na[PF_6]$ to the reaction mixture as a halide scavenger resulted in the formation of P,Sb-chelate complex **12** (Scheme 7), which could be separated from a minor, Ru-containing impurity by chromatography and isolated in 56% yield (in a partly solvated form).

Analogous reactions employing the isoelectronic precursor $[RhCl(\mu\text{-}Cl)(\eta^5\text{-}C_5Me_5)]_2$ did not yield any ligand-bridged dirhodium complex but instead spontaneously produced P,Sb-chelate complex **13a** (Scheme 7) irrespective of the Rh : **3** molar ratio (1 : 1 or 2 : 1), presumably due to the greater polarising power of the harder, formally trivalent Rh atom. Similar compound **13b** with a hexafluorophosphate counteranion was obtained when $Na[PF_6]$ was added to a mixture containing $[RhCl(\mu\text{-}Cl)(\eta^5\text{-}C_5Me_5)]_2$ and **3** (Rh : **3** = 1 : 1). Even in this case, the behaviour of **3** differed from that of dppf and **1**, which produced ligand-bridged dinuclear complexes at the M : L 2 : 1 ratio, while the formation of chelate complexes with these ligands required halide abstraction (*i.e.*, did not spontaneously proceed, such as with **3** and the Rh precursor).

Due to the asymmetry of their coordination sphere, the metal ions in **12** and **13a**,**b** were stereogenic. As the result,

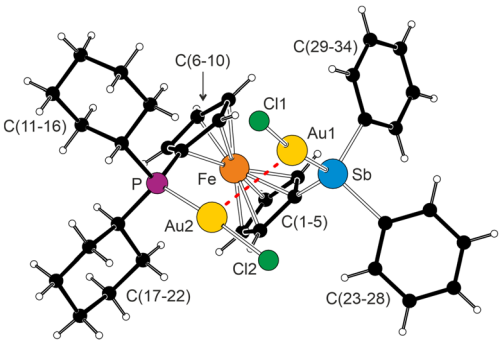

Fig. 6 Molecular structure of **11**. Selected distances and angles (in Å and deg.): Au1–Sb 2.4967(5), Au1–Cl1 2.2980(6), Sb–Au1–Cl 173.29(2), Au2–P 2.2349(5), Au2–Cl2 2.3019(5), and P–Au2–Cl2 171.58(3). The Au···Au interaction is indicated by a red dashed line.

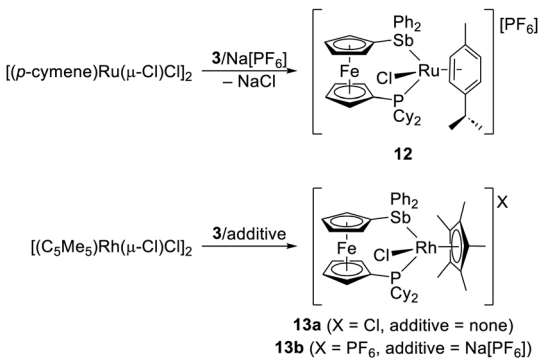

Scheme 7 Preparation of (arene)M complexes **12** and **13**.

eight distinct ^{1}H and ^{13}C NMR resonances were observed due to the diastereotopic ferrocene CH groups, and similar NMR responses were noted for the cyclohexyl and phenyl groups. The ^{31}P{^{1}H} NMR signal of **12** was observed as a singlet at δ_P 40.8 (coordination shift: δ_P = 48.2 ppm), and those of **13a** and **13b** were observed as doublets at δ_P 40.5 and 40.2 (δ_P = 48.0 and 47.7 ppm), respectively, due to coupling with ^{103}Rh ($I = \frac{1}{2}$, monoisotopic; $^{1}J_{RhP}$ = 136 Hz for both complexes).

The cations in the structures of **12**·$C_2H_4Cl_2$, **13a**·4$CHCl_3$ and **13b**·$C_2H_4Cl_2$ (Fig. 7 and Table 8) adopted similar piano stool geometries, which were slightly asymmetric due to dissimilar M–ligand distances (M–Sb > M–Cl/P) and varying steric demands of the donor moieties, which could be illustrated by the Cg^M–M–donor angles decreasing in the sequence Cg^M–M–P (131–132°) > Cg^M–M–Sb (125–128°) > Cg^M–M–Cl (118–123°; Cg^M stands for the centroid of the π-bound arene ligand). The individual M-donor distances were similar to the values reported for analogous complexes featuring **1** and dppf as chelating ligands.[6,45] Similar values (within a few degrees) were also found for the bite angles (Sb–M–P), which, however, seemed to be affected by the packing forces (*cf.* the values for **13a**·4$CHCl_3$ and **13b**·$C_2H_4Cl_2$). The ferrocene units in chelating **3** were eclipsed ($|\tau| < 7°$) and showed negligible tilting.

In contrast to experiments previously mentioned, reactions of **3** with [MCl_2(cod)] (M = Pd, Pt; cod = cycloocta-1,5-diene), as

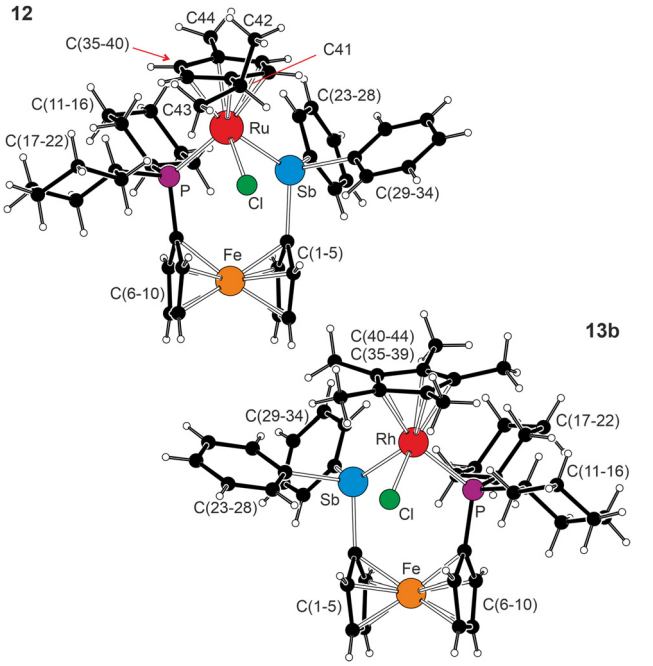

Fig. 7 Views of the complex cations in the structures of **12**·$C_2H_4Cl_2$ and **13b**·$C_2H_4Cl_2$ (for additional structure diagrams, see the ESI†).

Table 8 Selected distances and angles for **12**·$C_2H_4Cl_2$, **13a**·4$CHCl_3$ and **13b**·$C_2H_4Cl_2$ (in Å and deg.)

Parameter[a]	**12**·$C_2H_4Cl_2$	**13a**·4$CHCl_3$	**13b**·$C_2H_4Cl_2$
M	Ru	Rh	Rh
M–Cg^M	1.763(1)	1.859(1)	1.8625(9)
M–Sb	2.6074(5)	2.5787(4)	2.5913(4)
M–P	2.3882(6)	2.3725(7)	2.3700(5)
M–Cl	2.4026(8)	2.3998(7)	2.3967(9)
Sb–M–P	91.74(2)	94.53(2)	92.94(1)
Cl–M–Sb	79.47(2)	81.74(2)	82.21(2)
Cl–M–P	89.28(2)	89.18(2)	91.20(2)
∠Cp1,Cp2	1.6(2)	2.1(1)	2.3(1)
τ	3.8(2)	−6.5(1)	−3.0(1)

[a] Cg^M is the centroid of the π-coordinated aromatic ring (C(35–40) for the Ru complex and C(35–39) for both Rh complexes). Other parameters are defined the same as those for the free ligand (see footnote to Table 2).

MCl_2 synthetic proxies, proceeded uneventfully to give the expected P,Sb-chelate complexes **14** and **15** (Scheme 8) in approximately 70% yields after crystallisation.

The chelate structures of **14** and **15**, corroborated by structure determination (*vide infra*), were suggested by a low-field shift in the ^{31}P{^{1}H} NMR resonances, which were observed as singlets at δ_P 55.4 and 21.6, respectively, with the latter flanked by a pair of satellites due to the ^{195}Pt isotopomer ($I = \frac{1}{2}$, abundance: 34%; $^{1}J_{PtP}$ = 3608 Hz), and by shifts in the ^{13}C{^{1}H} NMR signals due to the Sb-substituted rings. Compound **14** was further characterised by splitting of the ^{13}C{^{1}H} NMR signal due to the ferrocene C^{ipso}-Sb into doublets by ^{31}P (δ_C 65.48, J_{PC} = 6 Hz).

Complexes [MCl_2(**3**-κ^{2}P,Sb)] (M = Pd and Pt) (Fig. 8) crystallised with similar structures but were not isostructural due to

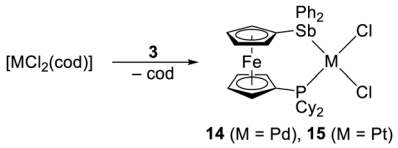

14 (M = Pd), **15** (M = Pt)

Scheme 8 Synthesis of Pd(II) and Pt(II) dichloride complexes **14** and **15** (cod = cycloocta-1,5-diene)

differences in solvation. The coordination environments of the Pd(II) and Pt(II) ions in these compounds were square planar, as expected, but were distorted with varying interligand angles and with the Cl2 atom displaced (by 0.367(1) Å and 0.165(1) Å in solvated **14** and **15**, respectively; *vide infra*) from the plane of the remaining atoms in the coordination sphere, {M, Cl1, P, Sb}, which, in turn, were coplanar within ≈0.04 Å. Even for **14** and **15**, the M-donor distances were similar to the values reported for similar complexes with the symmetrical ligands **1** and dppf. Similarly, the ligand bite angles (100° for **14**, and 98° for **15**), which were the largest among the interligand angles, did not differ from those in [$PdCl_2$(dppf-κ^{2}P,P′)] (98–99° for different solvates),[46] [$PdCl_2$(Cy_2PfcPCy_2-κ^{2}P,P′)] (102°),[16] [$PdCl_2$(Ph_2Pfc-PCy_2-κ^{2}P,P′)] (101°),[15] and [$PtCl_2$(dppf-κ^{2}P,P′)] (99°).[47] The ferrocene units adopted an intermediate conformation with τ = 28.2(2)° [16.6(1)°] (values for **14** [**15**]) and tilt angles of 5.1(1)° [4.1(1)°].

Although the structures of platinum metal complexes **12**–**15** were rather unexceptional, closer inspection of these complexes revealed minor structural distortions suggesting the presence of Cl → Sb interactions (most significantly in **12** and **14**; Fig. 9). In particular, the chloride ligands in the structures of the (arene)M complexes were slightly, albeit notably, bent towards the stibine group (Fig. 9), while in **14** and **15**, the chloride ligand adjacent to the stibine substituent (Cl2) was forced from the coordination plane towards Sb with concomitant closure of the Sb–M–Cl2 angle. The Sb···Cl distances were 3.2063(8) Å in solvated complex **12**, 3.2605(6)/3.2827(7) Å in **13a**/**13b**, and 3.2103(5)/3.1074(6) Å in **14**/**15**. In all cases, these distances were shorter than the sum of the van der Waals radii (Sb–Cl, 3.81 Å).[27b]

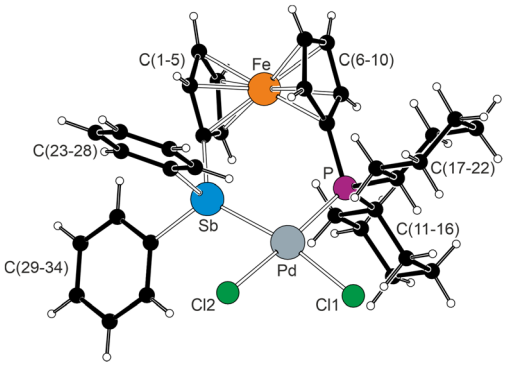

Fig. 8 View of the complex molecule in the structure of **14**·1.5CH_2Cl_2 (the structure diagram of **15**·1.5CH_2Cl_2 is available in the ESI†). Selected distances and angles (in Å and deg.) for **14**·1.5CH_2Cl_2 (M = Pd) [for **15**·CH_2Cl_2 in parentheses (M = Pt)]: M–Sb 2.4977(3) [2.5085(4)], M–P 2.2607(6) [2.2524(5)], M–Cl1 2.3380(6) [2.3441(5)], M–Cl2 2.3653(6) [2.3762(5)], Sb–M–P 100.44(2) [97.82(2)], Cl1–M–Cl2 90.53(2) [87.60(2)], Cl1–M–P 90.03(2) [92.21(2)], and Cl2–M–Sb 79.38(2) [82.13(2)].

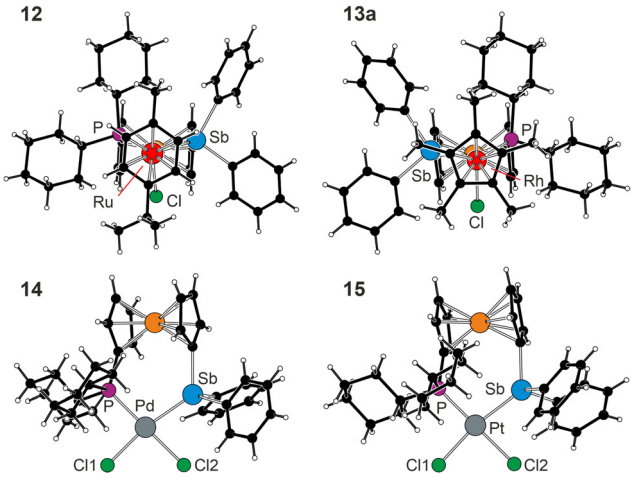

Fig. 9 Views of the complex cations in the structures of **12**·$C_2H_4Cl_2$ and **13a**·4$CHCl_3$ in the direction perpendicular to the π-arene ligand (top) and of the complex molecules in the structures of **14**·1.5CH_2Cl_2 and **15**·1.5CH_2Cl_2 in the direction perpendicular to the coordination plane. Selected angles (in deg.) for **12**·$C_2H_4Cl_2$: P–Ru–Cl 89.28(2), P–Ru–Sb 91.74(2), and Cl–Ru–Sb 79.47(2), and for **13a**·4$CHCl_3$ [**13b**·$C_2H_4Cl_2$]: P–Rh–Cl 89.18(2) [91.20(2)], P–Rh–Sb 94.53(2) [92.94(1)], and Cl–Rh–Sb 81.74(2) [82.21(2)].

To rule out a mere steric influence of the pnictogen substituents, the presumed Sb···Cl interaction was visualised using the noncovalent interaction analysis (NCI),[48] which is used to distinguish between repulsive and attractive weak contacts based on the reduced density gradient (RDG) plots. The attractive and repulsive contacts are discerned based on the magnitude of the sign(λ_2)ρ product, so that positive values correspond to repulsive contacts and negative values indicate attractive interactions. Indeed, the NCI analysis for model compounds **12** and **14** revealed regions of significantly negative sign(λ_2)ρ values between the Sb and Cl atoms (see Fig. S26, ESI†), indicating weak attractive interactions in both complexes.

Conclusions

In summary, this study further illustrates the remarkable properties of derivatives functionalised with phosphine and stibine groups arising from the different reactivities of their functional substituents, which mainly reflects the differing chemistries of pentavalent phosphorus and antimony. Particularly attractive is the possibility of independently altering the properties of the pnictogen groups in derivatives that combine phosphorus and antimony substituents, which is relatively easily achieved by changing their substituents and the oxidation state of their "central" atom. When properly combined, these manipulations can result in intramolecular P → Sb or P=E → Sb dative interactions between the Lewis basic phosphine or phosphine chalcogenide moieties and Lewis acidic stiboranes. As demonstrated here *via* a combination of

experimental and theoretical methods, the P → Sb interactions can be further fine-tuned through substituents at the phosphorus atom (*viz.*, the change observed for **8**-type compounds upon replacement of the phenyl substituents at the phosphorus atom by cyclohexyl groups; similar changes in the corresponding P-chalcogenides had only a minimal impact).

Additionally, the coordination behaviour of the mixed derivatives is different from that of the analogous symmetrical ligands. In P,Sb-donors such as **2** and **3**, the phosphine group acts as the primary donor site for soft metal ions, while the stibine moiety remains accessible for further modifications or coordination if additional metal ions or vacant coordination sites are available. In the case of Au(I) ions, the behaviour of **3** parallels that of distibine **1**, which differs from that of dppf. An entirely different reactivity is observed towards the (C_5Me_5)-Rh(III)Cl_2 fragment, where **3** favours the formation of cationic P,Sb-chelate complexes, whereas **1** and dppf form primarily symmetrical, ligand-bridged dinuclear complexes, and the formation of cationic chelates requires the presence of halide scavengers (which naturally facilitate reactions producing the P,Sb-chelate complexes even from **3**). Some complexes exhibit short Cl···Sb contacts in their structures, suggesting additional (weak) Sb–Cl interactions, in which the lone pair electron density at a terminal chloride ligand is partly donated to the Sb atom, whose Lewis acidity is enhanced by coordination to a metal centre.

Conflicts of interest

There are no conflicts of interest to declare.

Acknowledgements

The authors gratefully acknowledge the financial support from the Czech Science Foundation (project no. 21-02316S). Theoretical calculations were performed using the resources provided by the e-INFRA CZ project (ID: 90254), supported by the Ministry of Education, Youth and Sports of the Czech Republic.

References

1 Phosphorus(III) Ligands, in *Homogeneous Catalysis*, ed. P. C. J. Kamer and P. W. N. M. van Leeuwen, Wiley, Chichester, 2012.

2 (*a*) N. R. Champness and W. Levason, *Coord. Chem. Rev.*, 1994, **133**, 115; (*b*) W. Levason and G. Reid, *Coord. Chem. Rev*, 2006, **250**, 2565; (*c*) H. Werner, *Angew. Chem., Int. Ed.*, 2014, **43**, 938; (*d*) S. L. Benjamin and G. Reid, *Coord. Chem. Rev*, 2015, **297–298**, 168; (*e*) V. K. Greenacre, W. Levason and G. Reid, *Coord. Chem. Rev*, 2021, **432**, 213698; (*f*) J. M. Lipshultz, G. Li and A. T. Radosevich, *J. Am. Chem. Soc.*, 2021, **143**, 1699; (*g*) W. M. Hollingsworth and E. A. Hill, *J. Coord. Chem.*, 2022, **75**, 1436; (*h*) J. L. Wardell, Arsenic, Antimony and Bismuth, in *Comprehensive Organometallic Chemistry II*, ed. E. W. Abel, F. G. A. Stone and G. Wilkinson, Elsevier, Oxford, 1995, vol. 2, ch. 8, pp. 321–347; (*i*) W. Levason and G. Reid, Acyclic Arsine, Stibine, and Bismuthine Ligands, in *Comprehensive Coordination Chemistry II: From Biology to Nanotechnology*, ed. J. A. McCleverty and T. J. Meyer, Elsevier, Oxford, 2003, vol. 1, ch. 1.16, pp. 377–389.

3 (*a*) A. Togni and T. Hayashi, ed., *Ferrocenes: Homogeneous Catalysis, Organic Synthesis, Materials Science*, VCH, Weinheim, 1995; (*b*) P. Štěpnička, ed., *Ferrocenes: Ligands, Materials and Biomolecules*, Wiley, Chichester, 2008; (*c*) R. C. J. Atkinson, V. C. Gibson and N. J. Long, *Chem. Soc. Rev.*, 2004, **33**, 313; (*d*) R. Gómez Arrayás, J. Adrio and J. C. Carretero, *Angew. Chem., Int. Ed.*, 2006, **45**, 7674; (*e*) L. Cunningham, A. Benson and P. J. Guiry, *Org. Biomol. Chem.*, 2020, **18**, 9329; (*f*) P. Štěpnička, *Dalton Trans.*, 2022, **51**, 8085.

4 (*a*) P. Sharma, J. G. Lopez, C. Ortega, N. Rosas, A. Cabrera, C. Alvarez, A. Toscano and E. Reyes, *Inorg. Chem. Commun.*, 2006, **9**, 82; (*b*) J. Vázquez, P. Sharma, A. Cabrera, A. Toscano, S. Hernández, J. Pérez and R. Gutiérrez, *J. Organomet. Chem.*, 2007, **692**, 3486; (*c*) D. Pérez, P. Sharma, N. Rosas, A. Carbrera, J. L. Arias, F. del Rio-Portilla, J. Vazquez, R. Gutierrez and A. Toscano, *J. Organomet. Chem.*, 2008, **693**, 3357; (*d*) A. M. Ortiz, P. Sharma, D. Pérez, N. Rosas, A. Cabrera, L. Velasco, A. Toscano and S. Hernández, *J. Organomet. Chem.*, 2009, **694**, 2037; (*e*) D. Pérez, P. Sharma, A. Cabrera, N. Rosas, I. Arellano, A. Toscano and S. Hernández, *Polyhedron*, 2009, **28**, 3115; (*f*) D. Pérez, P. Sharma, A. M. Ortiz, A. Cabrera, S. Hernández, A. Toscano and R. Gutiérrez, *Z. Naturforsch.*, 2012, **67b**, 36; (*g*) D. Perez, C. Herrera, M. Sharma, R. Gutierrez, S. Hernández, A. Toscano and P. Sharma, *J. Organomet. Chem.*, 2013, **743**, 97.

5 An earlier report mentioned triferrocenylstibine, albeit without any synthetic or characterisation details: A. E. Ermoshkin, N. P. Makarenko and K. I. Sakodynskii, *J. Chromatogr.*, 1984, **290**, 377. Furthermore, a sterically stabilised distibene, Fc*Sb═SbFc* (Fc* = 2,5-bis(3,5-di-*t*-butylphenyl)ferrocenyl), was reported in: M. Sakagami, T. Sasamori, H. Sakai, Y. Furukawa and N. Tokitoh, *Chem. – Asian J.*, 2013, **8**, 690.

6 J. Schulz, J. Antala, I. Císařová and P. Štěpnička, *Dalton Trans.*, 2023, **52**, 1198.

7 (*a*) K.-S. Gan and T. S. A. Hor, 1,1′-Bis(diphenylphosphino)ferrocene. Coordination Chemistry, Organic Syntheses, and Catalysis, in *Ferrocenes: Homogeneous Catalysis, Organic Synthesis Materials Science*, ed. A. Togni and T. Hayashi, Wiley-VCH, Weinheim, Germany, 1995, ch. 1, pp. 3–104; (*b*) S. W. Chien and T. S. A. Hor, The Coordination and Homogeneous Catalytic Chemistry of 1,1′-Bis-(diphenylphosphino)ferrocene and its Chalcogenide Derivatives, in *Ferrocenes: Ligands, Materials and Biomolecules*, ed. P. Štěpnička, Wiley, Chichester, UK, 2008, ch. 2, pp. 33–116; (*c*) T. J. Colacot and S. Parisel, Synthesis, Coordination Chemistry and Catalytic Use of dppf Analogs, in *Ferrocenes: Ligands, Materials and Biomolecules*, ed. P. Štěpničkas, Wiley, Chichester, U.K., 2008, ch. 3, pp. 117–140; (*d*) G. Bandoli and A. Dolmella, *Coord. Chem. Rev.*, 2000, **209**, 161; (*e*) D. J. Young,

S. W. Chien and T. S. A. Hor, *Dalton Trans.*, 2012, **41**, 12655; (*f*) S. Dey and R. Pietschnig, *Coord. Chem. Rev.*, 2021, **437**, 213850.

8 J. Schulz, J. Antala, D. Rezazgui, I. Císařová and P. Štěpnička, *Inorg. Chem.*, 2023, **62**, 14028.

9 For representative examples of P,Sb-donors, see: (*a*) J. W. Dawson and L. M. Venanzi, *J. Am. Chem. Soc.*, 1968, **90**, 7229; (*b*) B. R. Higginson, C. A. McAuliffe and L. M. Venanzi, *Inorg. Chim. Acta*, 1971, **5**, 37; (*c*) W. Levason and C. A. McAuliffe, *Inorg. Chim. Acta*, 1974, **11**, 33; (*d*) W. Levason and C. A. McAuliffe, *Inorg. Chim. Acta*, 1976, **16**, 167; (*e*) H. H. Karsch and E. Witt, *J. Organomet. Chem.*, 1977, **529**, 151; (*f*) W. Levason, K. G. Smith, C. A. McAuliffe, F. P. McCullough, R. D. Sedgwick and S. G. Murray, *J. Chem. Soc., Dalton Trans.*, 1979, 1718; (*g*) L. R. Gray, A. L. Hale, W. Levason, F. P. McCullough and M. Webster, *J. Chem. Soc., Dalton Trans.*, 1983, 2573; (*h*) T. Kaufmann, R. Joußen, N. Klas and A. Vahrenhorts, *Chem. Ber.*, 1983, **116**, 473; (*i*) J. R. Black, W. Levason, M. D. Spicer and M. Webster, *J. Chem. Soc., Dalton Trans.*, 1993, 3129; (*j*) M. Manger, J. Wolf, M. Laubender, M. Teichert, D. Stalke and H. Werner, *Chem. – Eur. J.*, 1997, **3**, 1442; (*k*) M. Manger, O. Gevert and H. Werner, *Chem. Ber.*, 1997, **130**, 1529; (*l*) H. C. Jewiss, W. Levason, M. D. Spicer and M. Webster, *Inorg. Chem.*, 1987, **26**, 2102; (*m*) S. Yasuike, S. Kawara, S. Okajima, H. Seki, K. Yamaguchi and J. Kurita, *Tetrahedron Lett.*, 2004, **45**, 9135; (*n*) C. R. Wade and F. P. Gabbaï, *Angew. Chem., Int. Ed.*, 2011, **50**, 7369; (*o*) I.-S. Ke and F. P. Gabbaï, *Inorg. Chem.*, 2013, **52**, 7145; (*p*) J. S. Jones, C. R. Wade and F. P. Gabbaï, *Angew. Chem., Int. Ed.*, 2014, **53**, 8876; (*q*) I.-S. Ke, J. S. Jones and F. P. Gabbaï, *Angew. Chem., Int. Ed.*, 2015, **53**, 2633; (*r*) H. Yang and F. P. Gabbaï, *J. Am. Chem. Soc.*, 2015, **137**, 13425; (*s*) B. A. Chalmers, M. Bühl, K. S. A. Arachchige, A. M. Z. Slawin and P. Kilian, *Chem. – Eur. J.*, 2015, **21**, 7520; (*t*) B. A. Chalmers, C. B. E. Meigh, P. S. Nejman, M. Bühl, T. Lébl, J. D. Woollins, A. M. Z. Slawin and P. Kilian, *Inorg. Chem.*, 2016, **55**, 7117; (*u*) J. S. Jones and F. P. Gabbaï, *Chem. – Eur. J.*, 2017, **23**, 1136; (*v*) D. You and F. P. Gabbaï, *J. Am. Chem. Soc.*, 2017, **139**, 6843; (*w*) J. S. Jones, C. R. Wade, M. Yang and F. P. Gabbaï, *Dalton Trans.*, 2017, **46**, 5598; (*x*) S. Sen, I.-S. Ke and F. P. Gabbaï, *Organometallics*, 2017, **36**, 4224; (*y*) S. Furan, E. Hupf, J. Boidol, J. Brünig, E. Lork, S. Mebs and J. Beckmann, *Dalton Trans.*, 2019, **48**, 4504; (*z*) M. Piesch, F. P. Gabbaï and M. Scheer, *Z. Anorg. Allg. Chem.*, 2021, **647**, 266.

10 (*a*) L.-L. Lai and T.-Y. Dong, *J. Chem. Soc., Chem. Commun.*, 1994, 2347; (*b*) I. R. Butler and R. L. Davies, *Synthesis*, 1996, 1350.

11 The synthesis of **4** was performed as previously reported: P. Štěpnička and I. Císařová, *Dalton Trans.*, 2013, **42**, 3373.

12 J. Schraml, M. Čapka and V. Blechta, *Magn. Res. Chem.*, 1992, **30**, 544.

13 C. Baillie, L. Zhang and J. Xiao, *J. Org. Chem.*, 2004, **69**, 7779.

14 K. D. Reichl, C. L. Mandell, O. D. Henn, W. G. Dougherty, W. S. Kassel and C. Nataro, *J. Organomet. Chem.*, 2011, **696**, 3882.

15 P. Vosáhlo, I. Císařová and P. Štěpnička, *J. Organomet. Chem.*, 2018, **860**, 14.

16 L. E. Hagopian, A. N. Campbell, J. A. Golen, A. L. Rheingold and C. Nataro, *J. Organomet. Chem.*, 2006, **691**, 4890.

17 S. I. Kirin, H.-B. Kraatz and N. Metzler-Nolte, *Chem. Soc. Rev.*, 2006, **35**, 348.

18 (*a*) J. A. Davies, S. Dutremez and A. A. Pinkerton, *Inorg. Chem.*, 1991, **30**, 2380; (*b*) N. P. Taylor, J. A. Gonzalez, G. S. Nichol, A. García-Domínguez, A. G. Leach and G. C. Lloyd-Jones, *J. Org. Chem.*, 2022, **87**, 721; (*c*) Y. J. Tan, C. I. Yeo, N. R. Halcovitch, M. M. Jotani and E. R. T. Tiekink, *Acta Crystallogr., Sect. E: Crystallogr. Commun.*, 2017, **73**, 493.

19 The C–Sb–C angles in **3** and **3**·BH_3 (93.6(1)–96.5(1)° and 95.0(1)–96.8(1)°) vary significantly less than those in **3O** (90.71(6)–99.60(6)°) and **3S** (92.75(6)–99.42(6)°).

20 D. Cremer and J. A. Pople, *J. Am. Chem. Soc.*, 1975, **97**, 1354.

21 The oxidation of a stibine SbR_3 with $SOCl_2$ produces stiborane $SbCl_2R_3$ and ''SO'', which disproportionates into SO_2 and S: P. W. Schenk and R. Steudel, *Angew. Chem., Int. Ed. Engl.*, 1965, **4**, 402.

22 Compare the ^{31}P NMR chemical shift with the value reported for $Ph_2PC(O)fcPCy_2{\cdot}BH_2Cl$ (δ_P 8.1): P. Vosáhlo, I. Císařová and P. Štěpnička, *New J. Chem.*, 2022, **46**, 21536.

23 A. W. Addison, T. N. Rao, J. Reedijk, J. van Rijn and G. C. Verschoor, *J. Chem. Soc., Dalton Trans.*, 1984, 1349.

24 O. Bárta, I. Císařová, J. Schulz and P. Štěpnička, *New J. Chem.*, 2019, **43**, 11258.

25 Recently, it was shown that selective oxidation of the stibine moiety in phosphinostibines can be achieved with 3,5-di-*tert*-butyl-*o*-benzoquinone: B. Zhou, S. Bedajna and F. P. Gabbaï, *Chem. Commun.*, 2024, **60**, 192.

26 (*a*) H. Brisset, Y. Gourdel, P. Pellon and M. Le Corre, *Tetrahedron Lett.*, 1993, **34**, 4523; (*b*) J. M. Brunel, B. Faure and M. Maffei, *Coord. Chem. Rev.*, 1998, **178–180**, 665.

27 (*a*) B. Cordero, V. Gómez, A. E. Platero-Prats, M. Revés, J. Echeverría, E. Cremades, F. Barragán and S. Alvarez, *Dalton Trans.*, 2008, 2832; (*b*) M. Mantina, A. C. Chamberlin, R. Valero, C. J. Cramer and D. G. Truhlar, *J. Phys. Chem. A*, 2009, **113**, 5806.

28 R. R. Holmes, R. O. Day, V. Chandrasekhar and J. M. Holmes, *Inorg. Chem.*, 1987, **26**, 163.

29 R. F. W. Bader, *Chem. Rev.*, 1991, **91**, 893.

30 (*a*) J. Tomasi, B. Mennucci and R. Cammi, *Chem. Rev.*, 2005, **105**, 2999; (*b*) G. Scalmani and M. J. Frisch, *J. Chem. Phys.*, 2010, **132**, 114110.

31 (*a*) D. Cremer and E. Kraka, *Angew. Chem., Int. Ed. Engl.*, 1984, **23**, 627; (*b*) P. Macchi, D. M. Proserpio and A. Sironi, *J. Am. Chem. Soc.*, 1998, **120**, 13429; (*c*) P. Macchi and A. Sironi, *Coord. Chem. Rev.*, 2003, **238**, 383; (*d*) D. Stalke, *Chem. – Eur. J.*, 2011, **17**, 9264.

32 (*a*) R. Bianchi, G. Gervasio and D. Marabello, *Inorg. Chem.*, 2000, **39**, 2360; (*b*) E. Espinosa, I. Alkorta, J. Elguero and E. Molins, *J. Chem. Phys.*, 2002, **117**, 5529.

33 (*a*) D. B. Chesnut, *J. Am. Chem. Soc.*, 1999, **121**, 2335; (*b*) K. Yamada and N. Koga, *J. Comput. Chem.*, 2013,

34, 149; (*c*) B. Lindquist-Kleissler, J. S. Wenger and T. C. Johnstone, *Inorg. Chem.*, 2021, **60**, 1846.

34 (*a*) G. Knizia, *J. Chem. Theory Comput.*, 2013, **9**, 4834; (*b*) G. Knizia and J. E. M. N. Klein, *Angew. Chem., Int. Ed.*, 2015, **54**, 5518.

35 (*a*) C. Lindner, B. Maryasin, F. Richter and H. Zipse, *J. Phys. Org. Chem.*, 2010, **23**, 1036; (*b*) C. Lindner, R. Tandon, B. Maryasin, E. Larionov and H. Zipse, *Beilstein J. Org. Chem.*, 2012, **8**, 1406.

36 (*a*) J. C. Kotz and C. L. Nivert, *J. Organomet. Chem.*, 1973, **52**, 387; (*b*) B. Corain, B. Longato, G. Favero, G. Ajo, G. Pilloni, U. Russo and F. R. Kreissl, *Inorg. Chim. Acta*, 1989, **157**, 259; (*c*) G. Pilloni, B. Longato and B. Corain, *J. Organomet. Chem.*, 1991, **420**, 57; (*d*) J. Podlaha, P. Štěpnička, J. Ludvík and I. Císařová, *Organometallics*, 1996, **15**, 543; (*e*) C. Nataro, A. N. Campbell, M. A. Ferguson, C. D. Incarvito and A. L. Rheingold, *J. Organomet. Chem.*, 2003, **673**, 47.

37 (*a*) G. Gritzner and J. Kůta, *Pure Appl. Chem.*, 1984, **56**, 461; (*b*) R. R. Gagné, C. A. Koval and G. C. Lisensky, *Inorg. Chem.*, 1980, **19**, 2854.

38 C. Hansch, A. Leo and R. W. Taft, *Chem. Rev.*, 1991, **91**, 165.

39 The difference in the redox potentials determined for (diphenylphosphino)ferrocene and the corresponding phosphine oxide was approximately 120 mV in MeCN, see ref. 36*d*.

40 (*a*) A. Houlton, D. M. P. Mingos, D. M. Murphy, D. J. Williams, L.-T. Phang and T. S. A. Hor, *J. Chem. Soc., Dalton Trans.*, 1993, 3629; (*b*) L.-T. Phang, T. S. A. Hor, Z.-Y. Zhou and T. C. W. Mak, *J. Organomet. Chem.*, 1994, **469**, 253.

41 A. Houlton, D. M. P. Mingos, D. M. Murphy and D. J. Williams, *Acta Crystallogr., Sect. C: Struct, Chem*, 1995, **51**, 30.

42 D. T. Hill, G. R. Girard, F. L. McCabe, R. K. Johnson, P. D. Stupik, J. H. Zhang, W. M. Reiff and D. S. Eggleston, *Inorg. Chem.*, 1989, **28**, 3529.

43 (*a*) H. Schmidbaur and A. Schier, *Chem. Soc. Rev.*, 2008, **37**, 1931; (*b*) H. Schmidbaur and A. Schier, *Chem. Soc. Rev.*, 2012, **41**, 370.

44 (*a*) F. Canales, M. C. Gimeno, P. G. Jones, A. Laguna and C. Sarroca, *Inorg. Chem.*, 1997, **36**, 5206; (*b*) O. Crespo, M. C. Gimeno, P. G. Jones and A. Laguna, *Acta Crystallogr., Sect. C: Cryst. Struct. Commun.*, 2000, **56**, 1433; (*c*) N. Meyer, F. Mohr and E. R. T. Tiekink, *Acta Crystallogr., Sect. E: Struct. Rep. Online*, 2010, **66**, m168.

45 (*a*) S. B. Jensen, S. J. Rodger and M. D. Spicer, *J. Organomet. Chem.*, 1998, **556**, 151; (*b*) J.-F. Ma and Y. Yamamoto, *J. Organomet. Chem.*, 1999, **574**, 148.

46 (*a*) T. Hayashi, M. Konishi, Y. Kobori, M. Kumada, T. Higuchi and K. Hirotsu, *J. Am. Chem. Soc.*, 1984, **106**, 158; (*b*) I. R. Butler, W. R. Cullen, T. J. Kim, S. J. Rettig and J. Trotter, *Organometallics*, 1984, **4**, 972.

47 (*a*) D. A. Clemente, G. Pilloni, B. Corain, B. Longato and M. Tiripicchio-Camellini, *Inorg. Chim. Acta*, 1986, **115**, L9; (*b*) A. Muller, *Acta Crystallogr., Sect. E: Struct. Rep. Online*, 2007, **63**, m210; (*c*) G. M. de Lima, C. A. L. Filgueiras, M. T. S. Giotto and Y. P. Mascarenhas, *Trans. Met. Chem.*, 1995, **20**, 380.

48 (*a*) E. R. Johnson, S. Keinan, P. Mori-Sánchez, J. Contreras-García, A. J. Cohen and W. Yang, *J. Am. Chem. Soc.*, 2010, **132**, 6498; (*b*) E. Pastorczak and C. Corminboeuf, *J. Chem. Phys.*, 2017, **146**, 120901.